Numerical Simulation of a Helical Magnetic Microswimmer Motion in the Non-Newtonian Blood

Mohammad Jahromi Aliabad[1], Farnaz Jazini Dorcheh[1]*, Majid Ghassemi[1]

[1]Fuel Cells and Nano Systems (FCNS) Laboratory, Department of Mechanical Engineering, K.N. Toosi University of Technology, Tehran, Iran.

*Corresponding author. Email: jazini@email.kntu.ac.ir

Abstract: Magnetic helical micro/nano-robots is inspired by the structure of the Escherichia coli (E. coli) bacterium. Since low-power magnetic fields are harmless to cells and tissues, magnetic helical micro/nano-robots are promising as a medical tool especially for in vivo applications. One of the uses of micro/nanorobots is to deliver drugs to cancerous tumors with minimal side effects. The present study models the swimming motion of the magnetic micro-robot inside a microchannel filled with blood, as a non-Newtonian fluid, using the Stokes equations. The nonlinear coupled equations are solved by a finite element method based software. The results indicate that increasing the number of helix turns, with a cut-off value, causes the terminal velocity of the microswimmer to increase. It is also shown that increases in the helix pitch causes the terminal velocity of the microswimmer to increase. Moreover, studies on cylindrical, spherical, and elliptic microswimmer heads indicated that the elliptic head has the minimum transverse displacement which is almost negligible.

Keywords: Micro-robot, nano-robot, magnetic helical swimmers, computational fluid dynamics, non-Newtonian fluid.

1 Introduction

Due to their small size and high mobility, magnetic helical nano-robots have potential applications in various areas, including medicine [1]. Magnetic fields with low intensities are harmless to cells and tissues. Therefore, magnetic helical nano-robots are promising tools for medical applications, such as surgery, cell manipulation, and drug delivery [2, 3]. Inspired by the Escherichia coli (E. coli) bacterium, researchers have invented magnetic robots of helical shape [4]. Under a rotating magnetic field, these devices can convert a rotational motion into a translational one to propel themselves within a fluid medium [5]. According to Abbott et al. microswimmers with helical tails and flexible flagella perform better, are faster swimmers, and more efficient than robots that are directly controlled by the magnetic field gradient. By modifying the external magnetic field's direction and rotational frequency, it is possible to control microswimmers with helical tails [5].

In 1973, H. Berg demonstrated that various microorganisms, such as E. coli, rotate their helical flagella as a molecular motor to swim in liquids [6]. In 1996, Honda et al. proposed a helical mechanism for micro-robots moving in low-Reynolds environments and built the first prototype of a helical robot on a centimeter scale. This swimming robot consisted of a 1mm×1mm×1mm SmCo magnet connected to a helical copper wire. It was activated wirelessly via an external rotating magnetic field and proved its capability to swim in low-Re liquids by swimming in a highly viscous oil [7]. Their findings demonstrate that the forward speed of the swimmer increases

with the magnetic field frequency and overall helix length, reaching a maximum for the optimal wave number [7]. In 2005, the same group reduced the dimensions of the previously used helical robot to millimeters and demonstrated the potential of magnetic helical micro-robots to guide medical catheters in blood vessels [8]. The first prototype of a magnetic helical robot with artificial bacterial flagella was invented in 2007 at the Swiss Federal Institute of Technology in Zürich. This microswimmer had a soft magnetic head and a helical tail with a diameter of 3 mm and a length of 30-40 mm [9]. Then the movement and swimming behaviors of this magnetic helical robot in distilled water were investigated [9].

Because of the importance of understanding motion and optimizing the design of microrobots inside capillaries and blood vessels, experiments and theoretical research on artificial swimmers inside channels and near surfaces have garnered a lot of attention. Although there have been some research on natural microswimmers within channels [10, 11, 12, 13, 14, 15] and near solid boundaries [16, 17, 18], there have been few studies on bio-inspired artificial swimming microrobots. Giacche et al. employed a BEM model to investigate the entrapment of microorganisms with helical tails near planar walls. The numerical model fits very well with experimental observations, and the helical wavelength and amplitude have a substantial effect on the microorganism's stable trajectory [15]. Bacteria were shown to follow circular trajectories near solid boundaries that are affected by hydrodynamic processes [16, 17] and changed by Brownian forces that modify the organisms distance from the wall [18]. Berke et al. measured the distribution of E. coli swimming across glass plates and compared their data to a hydrodynamic model to explore the hydrodynamic interactions of swimming organisms with solid surfaces [19]. DiLuzio et al. conducted experiments on smooth swimming of Escherichia coli cells in rectangular channels with widths ranging from 1.3 to 1.5μm (slightly larger than the diameter of the organism's body) and discovered that some surfaces, such as agar rather than PDMS, are preferred by bacteria over others [13]. Using the boundary element method, Shum et al. improved the power efficiency of a bacterium driven by a single helical flagellum at a solid boundary in relation to the geometrical parameters of the cell body and the flagellum. The authors concluded that the shape of bacteria influences boundary accumulation; that is, bacteria might be attracted or repelled by solid boundaries owing to hydrodynamic interaction according to geometrical parameters of the body and flagellum [20]. Temel et al. investigated the movement of a helical magnetic microswimmer inside cylindrical glass tubes filled with glycerol using both experimental methods and computational models [21, 22]. It has been observed that there is a proportional relationship between the time-average velocity and the rotation frequency of the magnetic helical swimmers until the step-out frequency, and then the swimmer loses its coordination with the magnetic field due to the increase in viscous torque and forward velocity drops [21]. According to the computer model results based on CFD solutions of the Stokes equations, swimming near the wall is faster than swimming in the center [22]. Furthermore, the model demonstrated that rotating the helical tail creates a localized flow around the swimmer, resulting in stresses and torques that change the swimmer's orientation in the channel [22]. In 2014, Temel et al. moved a magnetic microswimmer in a rectangular channel containing glycerol and investigated the effects of rotational frequency and channel surface roughness on the swimmer's movement [23]. Ramia et al. examined the swimming of microorganisms with spherical bodies and rotating helical flagella using the BEM method for four distinct situations: in an unbounded medium, next to a plane boundary, in the middle of two parallel boundaries, and with other swimmers nearby. When the swimmer's

swimming velocity and angular velocity in an unbounded fluid are compared to the case with a planar boundary, a drop of less than 10% owing to flagellar locomotion is seen. Up to 10% of the

velocity can be lost due to interactions with parallel planar boundaries or other nearby swimmers [24]. In another study, Goto et al. [25] used the BEM method to study the back and forward motion of flagellated bacteria near a planar boundary and observed that swimming trajectories and velocities during the swimmer's back and forward motion due to the effects of the pitch angle and the angle between the boundary and the helical tail axis are different [25]. Felderhof [26] developed an analytical model for swimming infinite helices inside circular channels based on the geometry of the helical structure's first order expansion. In-channel swimming is faster and more efficient than unbounded swimming, especially for thick tails, according to the data [26]. A comprehensive overview and framework for hydrodynamic modeling of swimming organisms, including modeling of interactions between bodies and boundaries, were presented by Lauga and Powers in 2009 [27]. Zhang et al. created a helical filament from GaAs that was attached to a soft magnetic nickel body on one side and had dimensions of 1.8 μm in width, 30 μm in length, and 200 nm in thickness. The authors used a rotational magnetic field to demonstrate the structure moving forward in the direction of the helical axis and noted that linear swimming velocity was influenced by both the size of the magnetic head and the strength of the magnetic field [28]. Dreyfus et al. created a magnetic microswimmer and showed that the speed of the microswimmer depends on the oscillation frequency, the length and the elastic property of the helical of the swimmer [29]. In a solution of branched polymer chains, Berg and Turner's [30] research demonstrated that the angular velocity of the body of a tethered E. coli cell is inversely proportional to the fluid viscosity, supporting Newtonian dynamics. In contrast, the effect is less pronounced in the solution of unbranched polymer chains, indicating strong non-Newtonian effects in that situation. Martinez et al. demonstrated that the swimming dynamics are greatly impacted by the non-Newtonian fluid's microrheology rather than the properties at macroscales assumed in a classical continuum fluid model [31]. Henry et al. demonstrated that the swimming speed in a continuous viscoelastic fluid monotonically declines with rising Deborah number (De) for an infinitely long filament passing a helical travelling wave of small amplitude [32]. On the other hand, a helical filament with a large pitch angle has been shown to swim with a speed that depends non-monotonically on the Deborah number [33, 34]. Li and Spagnolie [35] investigated the motion of helical bodies with arbitrary cross sections by solving the Stokes equations in a helical coordinate system. They demonstrated that for helices of any cross-section and in a viscoelastic fluid, the speed of each mode of the small amplitude helical wave is proportional to the real part of the complex viscosity. This conclusion holds true even when swimming is restricted to a tube. Demir et al showed that nonlocal shear-thinning effects substantially enhance the helical propulsion [36]. Dasgupta et al. [37] investigated the speed of propulsion of waving sheets inserted in freely rotating cylinders. When compared to the Newtonian limit, elastic fluids with shear-thinning viscosities (carboxymethyl cellulose and polyethylene oxide) invariably result in a drop in locomotion speed. Alperen et al. simulated the motion of a helical magnetic microswimmer inside a circular channel containing liquid glycerol and obtained the microswimmer's linear and angular velocities [38].

In this study, the effects of the geometric parameters of the number of helix turns, the helix pitch and the head of the microswimmer in the swimmer's movement are investigated in order to provide a microswimmer that has the highest speed and the most stable movement for swimming in non-Newtonian blood flow. The swimming of the helical microrobot inside a blood-filled microchannel, as a non-Newtonian fluid, is modeled using Stokes equations, and then the discretized equations are solved using a finite element based software.

2 Problem statement

This schematic of the microswimmer and the microchannel filled with blood is depicted in Fig.1. As shown by Fig.1, the system consists of a cylindrical microchannel (acting as the blood vessel) and a helical object modeling the E. coli bacterium. The microswimmer is made up of a NdFeB magnetic cylindrical head and a copper helical tail. Moreover, the fluid inside the microchannel is non-Newtonian, obeys the generalized power law, and possesses the characteristics of blood. The details of the microswimmer parameters are displayed in Fig. 1. We considered the initial value of microswimmer parameters and microchannel dimensions based on Alperen's paper [38] and listed them in Table 1.

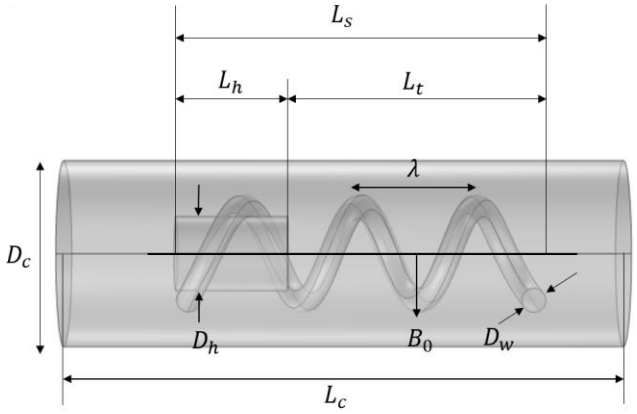

Fig. 1. Geometric parameters of the microswimmer

Table 1. Details of the initial microswimmer parameters and the microchannel dimensions

Description	Symbol	Parameter value
The head's diameter	D_h	400 µm
The head's length	L_h	600 µm
Wavelength of the helical tail	λ	625 µm
Radius of the helical tail	B_0	200 µm
The helix length	L_t	1250 µm
The helix diameter	D_w	130 µm
Total length of the microswimmer	L_s	1850 µm
Channel diameter	D_c	1000 µm
Channel length	L_c	3000 µm
Number of waves	n_λ	3
Frequency	f	1 Hz

3 Governing equations and boundary conditions

The governing continuity and the Navier-Stokes equations for an incompressible fluid are as follows, respectively:

$$\nabla.\mathbf{u_f} = 0 \tag{1}$$

$$\rho\left(\frac{\partial \mathbf{u_f}}{\partial t} + (\mathbf{u_f}.\nabla)\mathbf{u_f}\right) = -\nabla p + \mathbf{f} + \nabla.(\mu\nabla\mathbf{u_f}) \tag{2}$$

Where μ , $\mathbf{u_f}$, p , ρ , and $\mathbf{f}$ represent the dynamic viscosity, fluid velocity, pressure, density, and body force, respectively. Furthermore the Reynolds number used is based on the microswimmer diameter, as a length scale, and the tangential velocity of the microswimmer head, as the flow velocity, is determined as follow:

$$\mathrm{Re} = \frac{\rho V D}{\mu} = \frac{\rho \omega_x D_h^2}{2\mu} \tag{3}$$

Here, $\omega_x = 2\pi f$ denotes the angular velocity of the microswimmer along the x-direction, where f denotes the angular frequency and D_h represents the diameter of the microswimmer's head. Since the rotational frequency equals 1 Hz, the flow behaves as creeping flow because the Reynolds number is significantly smaller than 1. The governing equation representing the creeping flow in the microchannel is the simplified form of the Navier-Stokes equation and is as follow:

$$\nabla p = \mu\nabla^2\mathbf{u_f} + \mathbf{f} \tag{4}$$

To model the non-Newtonian behavior of blood, any of the Low Power, Casson, Carreau, and Generalized Power Law models can be used, but since in this problem, the shear stress rate is small, the best model to determine the non-Newtonian fluid behavior of blood is the Generalized Power Law model [39]. The Generalized Power Law model for modeling the non-Newtonian behavior of blood is as follows:

$$\mu = \lambda\,|\dot{\gamma}|^{n-1} \tag{5}$$

$$\lambda(|\dot{\gamma}|) = \mu_\infty + \Delta\mu\,\exp\left[-\left(1+\frac{|\dot{\gamma}|}{a}\right)\exp\frac{-b}{|\dot{\gamma}|}\right] \tag{6}$$

$$n(|\dot{\gamma}|) = n_\infty + \Delta n\exp\left[-\left(1+\frac{|\dot{\gamma}|}{c}\right)\exp\frac{-d}{|\dot{\gamma}|}\right] \tag{7}$$

Here, $|\dot{\gamma}|$ represents the strain rate. The other parameters are based on Ballyk et. al. [40] and are $\mu_\infty = 0.0035 Pa.s$, $n_\infty = 1$, $\Delta\mu = 0.025 Pa.s$, $\Delta n = 0.45$, $a = 50 s^{-1}$, $b = 3 s^{-1}$, $c = 50 s^{-1}$, and

$d = 4\,s^{-1}$ [39].

The boundary conditions are [38]:

1. The no-slip condition on the microchannel wall

2. The slip-free moving wall condition at the microswimmer's surface

3. The periodic boundary condition at the inlet and outlet of the channel

Although the pulsatile blood velocity should be included in the problem to have a comprehensive study; here, to avoid the complexity and convergence issues, since it was decided to find just the effects of geometrical parameters; following some other studies, the fluid velocity effects are not considered [22, 23, 38].

Since the Knudsen number for blood flow; based on the size of red blood cells, is about 0.336<1, the no-slip condition on the blood-microchannel and blood-microswimmer walls is justified [41]. The linear and angular velocity vectors is employed to calculate the local velocity at the moving boundary of the microswimmer. The moving wall boundary condition is defined as follow:

$$\mathbf{u} = \begin{bmatrix} U_{sw} \\ V_{sw} \\ W_{sw} \end{bmatrix} + \begin{bmatrix} \omega_x \\ \omega_y \\ \omega_z \end{bmatrix} \times \begin{bmatrix} x - x_{com} \\ y - y_{com} \\ z - z_{com} \end{bmatrix} \tag{8}$$

Where U_{sw}, V_{sw}, and W_{sw} represent the linear velocities and ω_x, ω_y, and ω_z denote the angular velocities of the microswimmer along the x-, y-, and z-directions, respectively. Furthermore, the x_{com}, y_{com}, and z_{com} represent the center of microswimmer mass.

In order to avoid burdening the calculations, the domain of solution (microchannel) should be considered small enough. Therefore, defining the periodic boundary conditions for the input and output of the microchannel, helps to have the domain of the problem in an expanded form.

The magnitude of the angular velocity component along the x-direction, ω_x, is known because of knowing the value of frequency *f*. On the other hand U_{sw}, V_{sw}, and W_{sw}, as well as ω_y and ω_z are unknown. Therefore five equations are needed to determine them. Two unknowns, the angular velocities ω_y and ω_z, are insignificant [22] and are considered to be zero. Therefore the number of unknown parameters reduces to three, which are determined from the force-free swimming condition by setting all fluid forces exerted on the microswimmer's surface equal to zero.

Since the net force exerted on the microswimmer by the fluid is determined by integrating the fluid stresses applied on the microswimmer surface, the force-free condition reads:

$$\mathrm{f_j} = \int_{\mathrm{S_{swimmer}}} \boldsymbol{\sigma_j}.\mathbf{n_s}\mathrm{ds} = 0 \tag{9}$$

Where $j = \{x, y, z\}$, $\boldsymbol{\sigma}$, and $\mathbf{n_s}$ represent the direction, fluid stress tensor, and the vector normal to the surface, respectively. Similar to force-free swimming condition, the moment-free swimming conditions are applied to determine the angular velocities along the y- and z-directions, as follows:

$$\tau_{\mathrm{y}} = \int_{\mathrm{S_{swimmer}}} \left[(z - z_{com})\boldsymbol{\sigma_x} - (x - x_{com})\boldsymbol{\sigma_z} \right] \mathbf{n_s}\mathrm{ds} = 0 \tag{10}$$

$$\tau_{\mathrm{z}} = \int_{\mathrm{S_{swimmer}}} \left[(x - x_{com})\boldsymbol{\sigma_y} - (y - y_{com})\boldsymbol{\sigma_x} \right] \mathbf{n_s}\mathrm{ds} = 0 \tag{11}$$

Where *x*, *y*, and *z* are coordinates of a point on the microswimmer's surface, and x_{com}, y_{com} and z_{com} denote the coordinates of the center of mass.

Equations (1), (4), (9), (10) and (11) with the mentioned boundary conditions were solved by Galerkin finite element method. The meshes were triangular and tetrahedral.

4 Numerical procedures

One of the methods for solving boundary value problems is the Galerkin finite element method [42, 43]. In this method, if you consider Ω as part of the spatial domain of the microchannel problem, the spatial domain in question is discretized by a large number of *Ns*, which are the vertices of the mesh elements. The domain is discretized by the mesh elements. Each n-vertex network is called a test function $\hat{g}_n$. The test function $\hat{g}_n$ is a linear function. Fig.2A is the front view of the microchannel and Fig.2B is part of the microchannel domain with a test function $\hat{g}_n$.

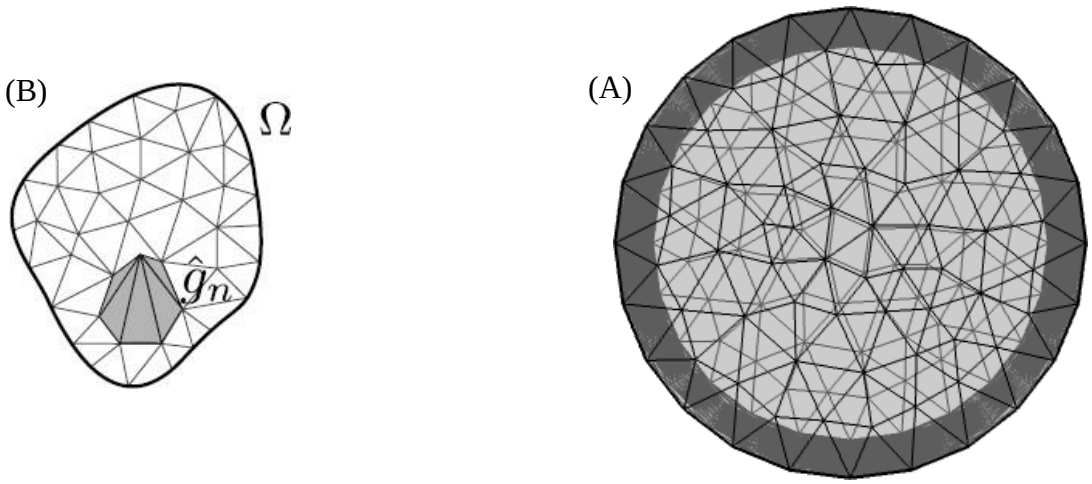

Fig. 2. Microchannel geometry. (A) View from the front of the microchannel. **(B)** Part of the microchannel domain.

As shown in Fig.2B, the test function $\hat{g}_n$ is located at the top of the n-shaped grid and the whole spatial domain is covered by the set of test functions $\{\hat{g}_n\}$. Each spatial domain $g(r)$ can be expressed as Eq. (12) according to the test function.

$$g(r) = \sum_n a_n \hat{g}_r \tag{12}$$

In the domain Ω, a boundary value problem can be defined as a differential equation in the form of Eq. (13).

$$\nabla . \mathbf{J} - \mathbf{F} = \mathbf{O} \tag{13}$$

In Eq. (13), ∇ is the differential operator, J is the problem equation, and F is the excitation function. In our problem, J is expressed by Eq. (14).

$$J = -\mathbf{P} + \mu \nabla \mathbf{u_f} \tag{14}$$

In Galerkin method, by multiplying the test function $\hat{g}_m(r)$ in Eq. (13) and integrating over the volume of the domain, the equation of weak form is obtained as Eq. (15).

$$\int_{\Omega} \hat{g}_m(r)\left[\ \nabla.J\left[g(r)\right]-F(r)=0\ \right]\ dV=0 \tag{15}$$

Using Eq. (12), the linear differential operator $J\left[g(r)\right]$ can be written as Eq. (16).

$$J\left[g(r)\right]=\sum_{n} a_n J\left[\hat{g}_n(r)\right] \tag{16}$$

The matrix form of Eq. (17) is obtained by placing Eq. (16) in Eq. (15).

$$\mathbf{K}\mathbf{a}=\mathbf{F} \tag{17}$$

In Eq. (17), the parameter $a=\{a_n\}$ is the coefficient of expansion, $\mathbf{K}$ is the stiffness matrix and $\mathbf{F}$ is the force vector. These values of $\mathbf{K}$ and $\mathbf{F}$ are in the form of Eq. (18) and (19), respectively.

$$k_{mn}=\int_{\Omega} \hat{g}_m(r)\ \nabla.\ J\left[\hat{g}_n(r)\right]\ dV \tag{18}$$

$$F_m=\int_{\Omega} \hat{g}_m(r)\ F(r)\ dV \tag{19}$$

Using finite element software, the discrete Eq. (17) with the mentioned boundary conditions is solved.

Verification

For verification, the resulting linear velocity of the microswimmer in glycerol as a function of the helix turns is compared with that of Alperen et al. [38]. As shown in Fig. 3, the results are in good agreement with the reference article. It must be noted that a negative velocity indicates that the microswimmer is swiming in a direction opposite to that of the default coordinates axis.

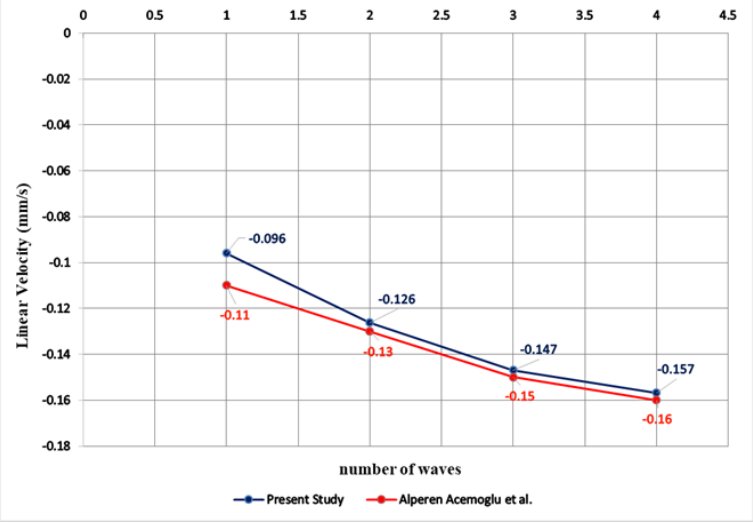

Fig. 3. The graph showing a comparison between the present work and the reference paper

Mesh independence

The mesh independence of the simulation results must be examined to ensure their validity. To this end, the mesh size must be refined up to a point at which the results converge. The convergence of the results indicates that the mesh is appropriate and may be used for the given equations and geometry. Since the aim of the present study is the investigation of the geometrical parameters of a microswimmer during forward motion for drug delivery to a cancerous tumor, the mesh independence was considered in terms of the microswimmer's velocity with respect to time.

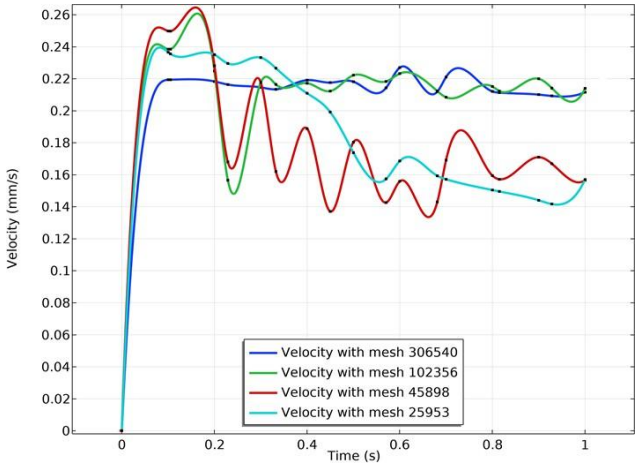

Fig. 4. Mesh independence graph

Mesh sizes of 25952, 45898, 102356, and 306540 were used to study mesh independence. As shown in Fig. 4, the graph of linear velocity versus time converges to 0.22 with an increase in the mesh size for an angular velocity of 2π. This graph changes to a line with an almost zero slope after the time 0.1s for a mesh size of 306540. Hence, we used a mesh size of 306540 for the solution. The mesh with a size of 306540 looks like the Fig. 5.

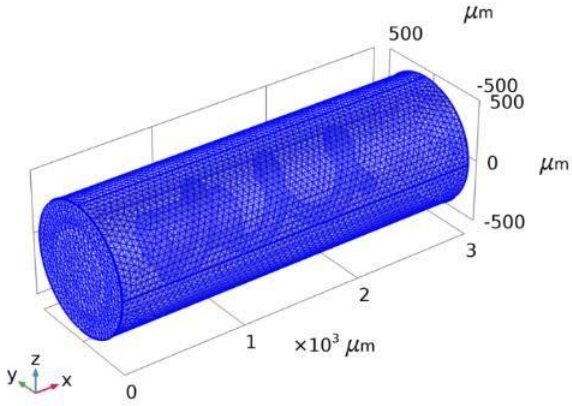

Fig. 5. The finite element mesh distribution on the surface and volume of the microchannel and the microswimmer

5 Results and discussion

In this section the effects of the geometric parameters of the microswimmer, namely the body shape, number of helix turns, and pitch of the helix, on the forward displacement and velocity of the microswimmer are studied in order to determine the optimal shape of a microswimmer swimming through blood flow with the aim of delivering drugs to a cancerous tumor.

To this end, a cylindrical microswimmer with a head length of 600 µm, a head diameter of 400 µm, and 3 helix turns at the center of the microchannel was considered as a reference. The geometry of the reference microswimmer selected to study the geometric parameters is shown in Fig. 6. The frequency of the rotating magnetic field was considered to be 1 Hz in all the simulations in order for the angular velocity of the microswimmer, which obeys $\omega_x = 2\pi f$, to remain constant. Moreover, the microswimmer is at the center of the microchannel containing non-Newtonian blood.

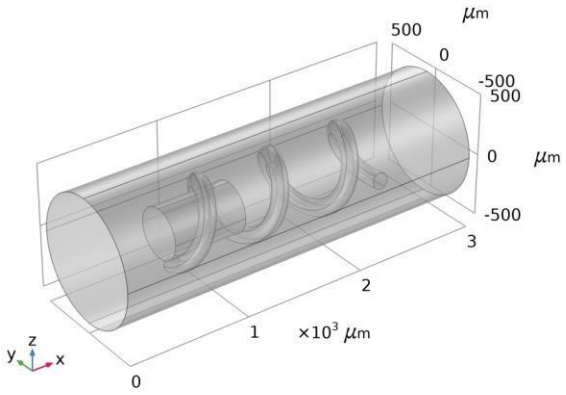

Fig. 6. A schematic of the reference geometry used to study the geometric parameters of the microswimmer

Number of helix turns

To examine the effect of the number of helix turns on the linear displacement and velocity of the microswimmer one to four turns were considered for the helix turns with a pitch of 625 µm. Fig. 7 displays the linear velocity components of the microswimmer for 1, 2, 3, and 4 turns in the helix. According to the figure, a rise in the number of turns up to 3 increases the forward terminal velocity of the microswimmer (U_{sw}), while a further increase in the number of turns decreases the velocity.

The terminal velocities of the microswimmer are $0.13\frac{mm}{s}$, $0.18\frac{mm}{s}$, $0.22\frac{mm}{s}$, and $0.20\frac{mm}{s}$ for 1, 2, 3, and 4 turns, respectively.

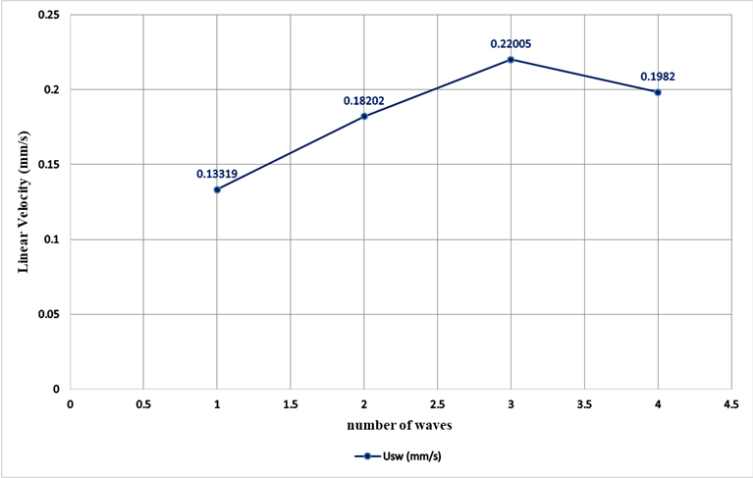

Fig. 7. The graph of changes in the forward linear velocity of the microswimmer for 1 to 4 turns in the helix

Helix pitch of the microswimmer

The terminal velocity of the microswimmer was determined for pitch values of 525 µm, 575 µm, 625 µm, 675 µm, 725 µm, 775 µm, and 825 µm in order to study the impact of this parameter. A plot of the terminal velocity versus the helix pitch in Fig. 8, indicates a linear increase in terminal velocity with a rise in the helix pitch. The microswimmer with 3 helix turns experienced an increase in terminal velocity less than $0.05\ \frac{mm}{s}$ for a 50 µm increase in the helix pitch. The terminal velocities corresponding to the smallest and largest helix pitches considered were $0.158\ \frac{mm}{s}$ and $0.309\ \frac{mm}{s}$, respectively.

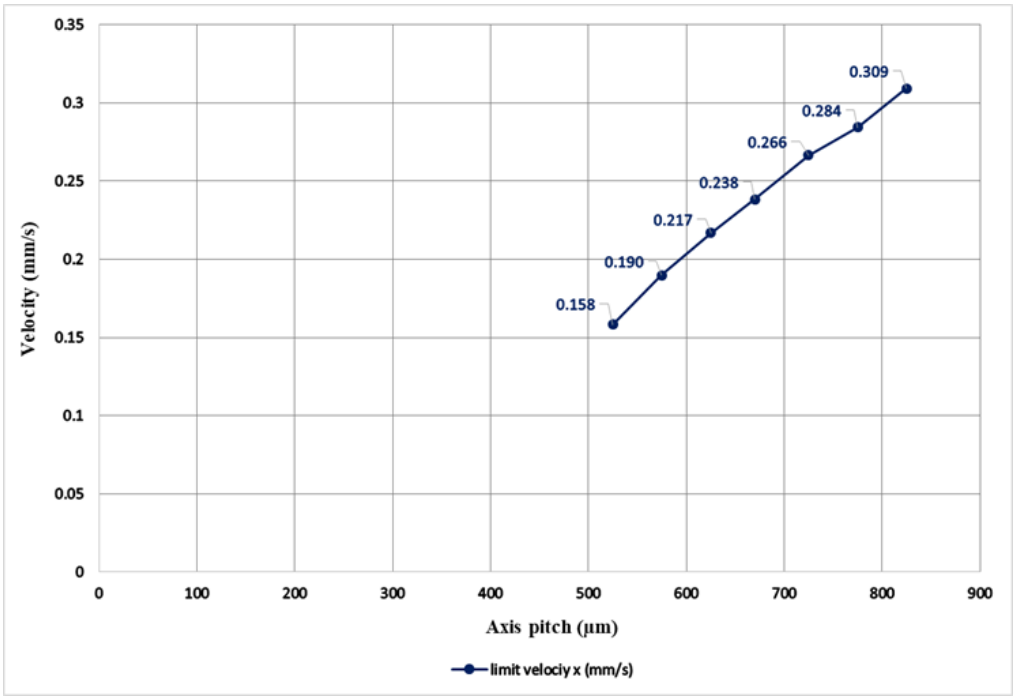

Fig. 8. The graph of the forward linear velocity of the microswimmer versus its helix pitch

Microswimmer head

Cylindrical, spherical, and elliptic head shapes were investigated in order to reduce the drag force on the head of the microswimmer optimized with respect to the number of helix turns. A comparison between the x-direction displacements demonstrated that the smallest displacement corresponded to the spherical head. This is due to the pressure drag exerted on the head. Moreover, the displacements corresponding to the cylindrical and elliptic heads were almost identical with the difference being that the displacements along the y- and z-directions were almost zero for the elliptic microswimmer. The displacement graphs are shown in Figs 9-11, for the spherical, elliptic and cylindrical head shapes, respectively.

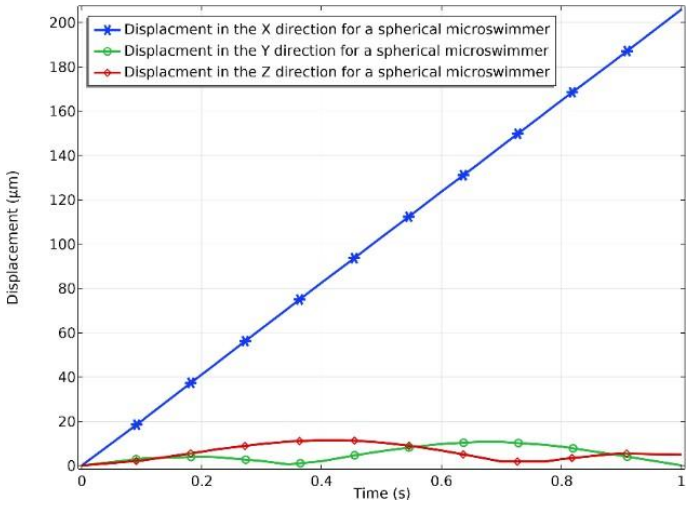

Fig. 9. The displacement-time graph of the microswimmer with the spherical head

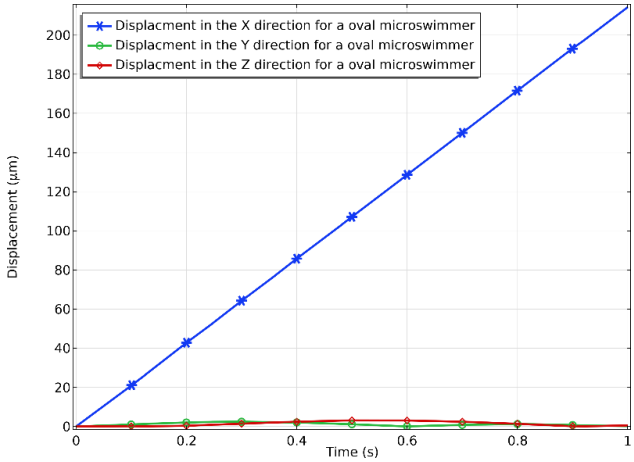

Fig. 10. The displacement-time graph of the microswimmer with the elliptic head

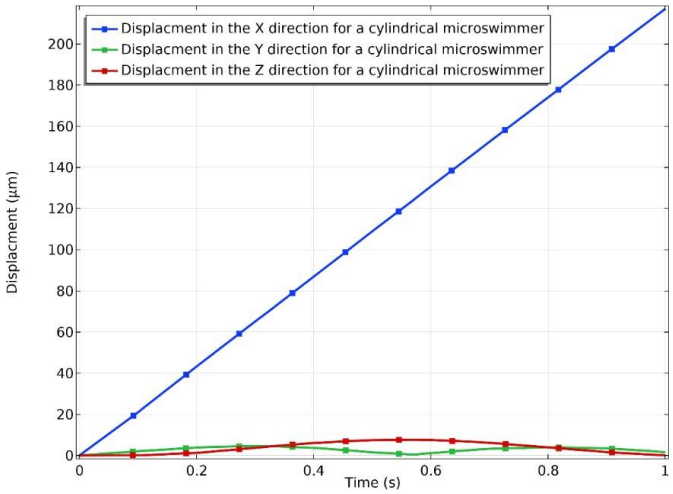

Fig. 11. The displacement-time graph of the microswimmer with the cylindrical head

6 Conclusion

In this study, the motion of a microswimmer inside a microchannel is numerically simulated to investigate the effects of geometric parameters of the microswimmer. The following overall conclusions can be drawn:

1. A study of the geometric parameters of the microswimmer indicated that the number of helix turns is a major parameter affecting the forward displacement and velocity of the microswimmer. With the omission of the microswimmer's tail, the magnetic cylinder was observed to move only about 3 μm. Furthermore, the microswimmer underwent its largest displacement, about 220 μm, for 3 helix turns. In addition, there is a cut-off value for helix turns after which the velocity of the microswimmer decreases with the increase of turns.

2. As the helix pitch was increased from 525 μm to 825 μm with 50 μm increments, the terminal velocity of the microswimmer increased from $0.158\frac{\text{mm}}{\text{s}}$ to $0.309\ \frac{\text{mm}}{\text{s}}$ with an approximate rate of $0.05\ \frac{\text{mm}}{\text{s}}$.

3. Spherical, cylindrical, and elliptic head shapes were investigated, and it was observed that the microswimmer with the elliptic head exhibited smaller displacements along the y- and z-directions due to a reduction in the pressure drag compared to those with the spherical and cylindrical shapes.

Declarations and statements

Funding: The authors declare that no funds, grants, or other support were received during the preparation of this manuscript.

Competing interests: Authors declare that they have no competing interests.

Data availability: All data are available in the main text.

Author contributions: The study is supervised and conceptualized by Majid Ghassemi. Design, Material preparation and data collection are performed by Mohammad Jahromi Aliabad.

Methodology and investigation is performed by Mohammad Jahromi Aliabad, Farnaz Jazini Dorcheh. The first draft of the manuscript was written by Mohammad Jahromi Aliabad and all authors commented on previous versions of the manuscript. All authors read and approved the final manuscript.

Ethics approval: Not applicable

Consent to participate: Not applicable

Consent for publication: Not applicable

References

[1] B. J. Nelson, I. K. Kaliakatsos and J. J. Abbott, "Microrobots for minimally invasive medicine," *Annu Rev Biomed Eng.*, pp. 12:55-85, 2010 Aug 15.

[2] K. E. Peyer, S. Tottori, F. Qiu, L. Zhang and B. J. Nelson, "Magnetic helical micromachines," *Chemistry*, vol. 19, no. 1, pp. 28-38, 2 Jan 2013 Jan 2.

[3] K. E. Peyer, L. Zhang and B. J. Nelson, "Bio-inspired magnetic swimming microrobots for biomedical applications," *Nanoscale*, vol. 5, no. 4, pp. 1259-1272, 2013.

[4] F. Qiu and B. J. Nelson, "Magnetic Helical Micro- and Nanorobots: Toward Their Biomedical Applications," *Engineering*, vol. 1, no. 1, pp. 021-026, 2015.

[5] J. J. Abbott, K. E. Peyer, M. C. Lagomarsino, L. Zhang, L. Dong, I. K. Kaliakatsos and B. J. Nelson, "How Should Microrobots Swim?," *The International Journal of Robotics Research*, vol. 28, no. 11-12, pp. 1434-1447, 2009.

[6] H. BERG and R. ANDERSON, "Bacteria Swim by Rotating their Flagellar Filaments," *Nature*, no. 245, p. 380–382, 1973.

[7] T. Honda, K. I. Arai and K. Ishiyama, "Micro swimming mechanisms propelled by external magnetic fields," *IEEE Transactions on Magnetics*, vol. 32, no. 5 PART 2, pp. 5085--5087, 1996.

[8] K. Kikuchi, A. Yamazaki, M. Sendoh, K. Ishiyama and K. I. Arai, "Fabrication of a spiral type magnetic micromachine for trailing a wire," *IEEE Transactions on Magnetics*, vol. 41, no. 10, pp. 4012-4014, 2005.

[9] D. J. Bell, S. Leutenegger, K. M. Hammar, L. X. Dong and B. J. Nelson, "Flagella-like Propulsion for Microrobots Using a Nanocoil and a Rotating Electromagnetic Field," in *Proceedings 2007 IEEE International Conference on Robotics and Automation*, 2007.

[10] H.C.Berg and L.Turner, "Chemotaxis of bacteria in glass capillary arrays. Escherichia coli, motility, microchannel plate, and light scattering," *Biophysical Journal*, vol. 58, no. 4, pp. 919-930, 1990.

[11] Z. Liu and K. D. Papadopoulos, "Unidirectional motility of Escherichia coli in restrictive capillaries," *Applied and Environmental Microbiology*, vol. 61, no. 10, p. 3567–72, 1995.

[12] S. A. Biondi, J. A. Quinn and H. Goldfine, "Random motility of swimming bacteria in restricted geometries," *AIChE journal*, vol. 44, no. 8, pp. 1923-1929, 1998.

[13] W. R. DiLuzio, L. Turner, M. Mayer, P. Garstecki, D. B. Weibel and H. C. B. &. G. M. Whitesides, "Escherichia coli swim on the right-hand side," *Nature*, vol. 435, p. 1271–1274, 2005.

[14] J. Männik, R. Driessen, P. Galajda, J. E. Keymer and a. C. Dekker, "Bacterial growth and motility in sub-micron constrictions," *Proceedings of the National Academy of Sciences of the United States of America*, vol. 106, no. 35, pp. 14861-14866, 2009.

[15] D. Giacché, T. Ishikawa and a. T. Yamaguchi, "Hydrodynamic entrapment of bacteria swimming near a solid surface," *APS physics*, vol. 82, no. 5, 2010.

[16] M. A.-S. Vigeant, R. M. Ford, M. Wagner and L. K. Tamm, "Reversible and Irreversible Adhesion of Motile Escherichia coli Cells Analyzed by Total Internal Reflection Aqueous Fluorescence Microscopy," *Applied and Environmental Microbiology*, vol. 68, no. 6, 2002.

[17] E. Lauga, W. R.DiLuzio, G. M.Whitesides and H. A.Stone, "Swimming in Circles: Motion of Bacteria near Solid Boundaries," *Biophysical Journal*, vol. 90, no. 2, pp. 400-412, 2006.

[18] G. Li, L.-K. Tam and a. J. X. Tang, "Amplified effect of Brownian motion in bacterial near-surface swimming," *Proceedings of the National Academy of Sciences of the United States of America*, vol. 105, no. 47, pp. 18355-18359, 2008.

[19] A. P. Berke, L. Turner, H. C. Berg and a. E. Lauga, "Hydrodynamic Attraction of Swimming Microorganisms by Surfaces," *Physical Review Letters*, vol. 101, no. 3, 2008.

[20] H. Shum, E. A. Gaffney and a. D. J. Smith, "Modelling bacterial behaviour close to a no-slip plane boundary: the influence of bacterial geometry," *Royal Society*, vol. 466, no. 2118, 2010.

[21] F. Z. Temel and S. Yesilyurt, "Magnetically actuated micro swimming of bio-inspired robots in mini channels," *IEEE*, pp. 342-347, 2011.

[22] F. Z. Temel and a. S. Yesilyurt, "Simulation-based analysis of micro-robots swimming at the center and near the wall of circular mini-channels," *Microfluidics and Nanofluidics*, vol. 14, no. 1, p. 287–298, 2013.

[23] F. Z. Temel and a. S. Yesilyurt, "Confined swimming of bio-inspired microrobots in rectangular channels," *Bioinspiration & Biomimetics*, vol. 10, no. 1, 2015.

[24] M.Ramia, D.L.Tullock and N.Phan-Thien, "The role of hydrodynamic interaction in the locomotion of microorganisms," *Biophysical Journal*, vol. 65, no. 2, pp. 755-778, 1993.

[25] TomonobuGoto, K. Nakata, K. Baba, M. Nishimura and Y. Magariyama, "A Fluid-Dynamic Interpretation of the Asymmetric Motion of Singly Flagellated Bacteria Swimming Close to a Boundary," *Biophysical Journal*, vol. 89, no. 6, pp. 3771-3779, 2005.

[26] B. U. Felderhof, "Swimming at low Reynolds number of a cylindrical body in a circular tube," *Physics of Fluids*, vol. 22, p. 113604 , 2010.

[27] E. Lauga and a. T. R. Powers, "The hydrodynamics of swimming microorganisms," *Reports on Progress in Physics*, vol. 72, no. 9, 2009.

[28] L. Zhang, J. J. Abbott, L. Dong, K. E. Peyer, B. E. Kratochvil, H. Zhang, C. Bergeles and a. B. J. Nelson, "Characterizing the Swimming Properties of Artificial Bacterial Flagella," *Nano Letters*, vol. 9, no. 10, p. 3663–3667, 2009.

[29] R. Dreyfus, J. Baudry, M. L. Roper, M. Fermigier and H. A. S. &. J. Bibette, "Microscopic artificial swimmers," *Nature*, vol. 437, no. 6, p. 862–865, 2005.

[30] H. C. BERG and &. L. TURNER, "Movement of microorganisms in viscous environments," *Nature* , vol. 278, p. 349–351, 1979.

[31] V. A. Martinez, J. Schwarz-Linek, M. Reufer, L. G. Wilson, A. N. Morozov and a. W. C. K. Poon, "Flagellated bacterial motility in polymer solutions," *Proceedings of the National Academy of Sciences,* vol. 111, no. 50, pp. 17771-17776, 2014.

[32] H. C. Fu, C. W. Wolgemuth and a. T. R. Powers, "Swimming speeds of filaments in nonlinearly viscoelastic fluids," *Physics of Fluids,* vol. 21, no. 3, 2009.

[33] B. Liu, T. R. Powers and a. K. S. Breuer, "Force-free swimming of a model helical flagellum in viscoelastic fluids," *Proceedings of the National Academy of Sciences,* vol. 108, no. 49, pp. 19516-19520, 2011.

[34] S. E. Spagnolie, B. Liu and a. T. R. Powers, "Locomotion of Helical Bodies in Viscoelastic Fluids: Enhanced Swimming at Large Helical Amplitudes," *physical review letters,* vol. 111, no. 6-9, 2013.

[35] L. Li and a. S. E. Spagnolie, "Swimming and pumping by helical waves in viscous and viscoelastic fluids," *Physics of Fluids,* vol. 27, no. 2, 2015.

[36] E. Demir, N. Lordi, Y. Ding and a. O. S. Pak, "Nonlocal shear-thinning effects substantially enhance helical propulsion," *Physical Review Fluids,* vol. 5, no. 11, 2020.

[37] M. Dasgupta, B. Liu, H. C. Fu, M. Berhanu, K. S. Breuer, T. R. Powers and a. A. Kudrolli, "Speed of a swimming sheet in Newtonian and viscoelastic fluids," *Physical Review E,* vol. 87, no. 1, 2013.

[38] A. Acemoglu, F. Z. Temel and S. Yesilyurt, "Characterization and Modeling of Micro Swimmers With Helical Tails and Cylindrical Heads Inside Circular Channels," *Journal of Fluids Engineering,* vol. 136, no. 12, Sep 2014.

[39] I. Husain, F. Labropulu, C. Langdon and a. J. Schwark, "A comparison of Newtonian and non-Newtonian models for pulsatile blood flow simulations," *Journal of the Mechanical Behaviour of Materials,* vol. 21, no. 5-6, p. 147–153, 2013.

[40] P. D. Ballyk, D. A. Steinman and C. R. Ethier, "Simulation of non-Newtonian blood flow in an end-to-side anastomosis," *Biorheology,* vol. 31, no. 5, pp. 565-86, Sep-Oct 1994.

[41] M. HOSAKA, T. NAGATA, S. TAKAHASHI and &. K. FUKUDA, "Numerical Simulation On Solid–liquid Multiphase Flow Including Complex-shaped Objects With Collision And Adhesion Effects Using Immersed Boundary Method," *International Journal of Computational Methods and Experimental Measurements,* vol. 6, no. 1, p. 13, 2018.

[42] S. Repin, "One Hundred Years of the Galerkin Method," *Computational Methods in Applied Mathematics,* vol. 17, no. 3, 2017.

[43] X. Wang, Y. Zou and Q. Zhai, "An effective implementation for Stokes Equation by the weak Galerkin finite element method," *Journal of Computational and Applied Mathematics,* vol. 370, no. 0377-0427, p. 112586, 2020.